JGR Space Physics

RESEARCH ARTICLE
10.1029/2019JA026667

Investigation on the Variability of the Geomagnetic Daily Current During Sudden Stratospheric Warmings

Charles Owolabi[1,2], Jiuhou Lei[1,3], O. S. Bolaji[4,5], Oluwaseyi Jimoh[1,6], Haibing Ruan[1], Na Li[1,7], Xiaojuan Niu[8], and Akimasa Yoshikawa[9]

[1]CAS Key Laboratory of Geospace Environment, School of Earth and Space Sciences, University of Science and Technology of China, Hefei, China, [2]Department of Physics, Federal University of Technology Akure, Nigeria, [3]CAS Center for Excellence in Comparative Planetology, Hefei, China, [4]Department of Physics, University of Lagos, Lagos, Nigeria, [5]Department of Physics, University of Tasmania, Hobart, Australia, [6]Department of Physics, Adeleke University, Ede, Nigeria, [7]National Key Laboratory of Electromagnetic Environment, China Research Institute of Radio-wave Propagation, Qingdao, China, [8]School of Physics and Information Engineering, Jianghan University, Wuhan, China, [9]International Center for Space Weather Science and Education, Kyushu University, Fukuoka, Japan

Key Points:
- Varying patterns of the zonal mean wind in the stratosphere play a major role in modulating the equatorial electrojet current strength
- Counter electrojet occurrence is noticeable during the sudden stratospheric warming as compared to the precondition period
- The lunar tide can be larger than the solar tide in electrojet current strength during the sudden stratospheric warming

Correspondence to:
J. Lei,
leijh@ustc.edu.cn

Citation:
Owolabi, C., Lei, J., Bolaji, O. S., Jimoh, O., Ruan, H., Li, N., et al. (2019). Investigation on the variability of the geomagnetic daily current during sudden stratospheric warmings. *Journal of Geophysical Research: Space Physics*, *124*, 6156–6172. https://doi.org/10.1029/2019JA026667

Received 28 FEB 2019
Accepted 25 JUN 2019
Accepted article online 2 JUL 2019
Published online 16 JUL 2019

Abstract The magnetic field records of the magnetometer networks in the American, East Asian-Australian, and European-African sectors were employed in this present work. We used them to investigate equatorial electrojet (EEJ), counter electrojet (CEJ), tidal variability in EEJ strength and ionospheric current during the 2005/2006 and 2008/2009 sudden stratospheric warming (SSW) events. In addition to the well-investigated tidal variability in EEJ strength over the American and East Asian sectors, we investigated that of the African sector for the first time. Interestingly, the tidal components in EEJ strength during both SSW events clearly exhibit marked longitudinal differences with high, moderate, and low amplitudes in the American, East Asian, and African sectors, respectively. An exception found around day 71 in the African sector after the 2008/2009 SSW event had higher solar diurnal tidal component as compared to that of the Asian sector. Over the American sector, solar and lunar semidiurnal tides were strongly associated with CEJ current during both SSW events, whereas at the African and East Asian sectors such variabilities are not evident. A solar diurnal tidal component was strongly related to a reduction in the EEJ strength over the East Asian sector. In addition, a prolonged period of CEJ occurrence that begins during the SSW precondition and ends when the SSW was evolving characterized the African sector during both SSW events. There is a steady shift in phase at later hours when both SSW events are evolving.

1. Introduction

The upper atmospheric winds play a significant role in the dynamics and electrodynamics of the low- and middle-latitude ionosphere (Anderson et al., 2004; Richmond, 1995). Under geomagnetically quiet conditions, the geomagnetic field exhibits a regular daily pattern in the dynamo region (~100- to 150-km altitude), which is often called solar quiet (*Sq*) variation in the dayside. At low and middle latitudes, neutral winds, which are the primary source of the *Sq* current system, are dominated by the upper atmospheric tides. These tidal winds, which are mainly due to the solar heating, force the electrically conducting fluid to move through the geomagnetic main field. This dynamo action produces an electromotive force, which in turn generates electric fields and currents in the ionosphere.

The morphology of this *Sq* current system that flows in each hemisphere takes the form of two large-scale vortices in the daylight region of each hemisphere. The direction of the current flow is anticlockwise in the Northern Hemisphere and clockwise in the Southern Hemisphere. In addition, the focus of a current system is at the center of circulation of the current loops (Pedatella et al., 2011; Yamazaki et al., 2011). On the other hand, observation of lunar daily geomagnetic variations (*L*) has revealed regular variation in the dynamo region of ionosphere (Yamazaki et al., 2011). The variation is attributed to the ionospheric current system generated by the atmospheric lunar tides due to the gravitational forces of the Moon and propagates to the upper atmosphere (Lindzen & Chapman, 1969; Yamazaki et al., 2012). The dominant wind component that causes *L* current variation is the semidiurnal lunar tide. The *L* semidiurnal tide variation (with period 12.42 hr) is small in magnitude compared to the corresponding solar semidiurnal variation (with period 12 hr). During the dayside sector, *L* is strongly enhanced, while it is significantly reduced

during the nighttime sector. However, the *L* current exhibits, in addition, a modulation depending on the lunar phase and can be separated from solar tides (Yamazaki et al., 2012; Yamazaki, Richmond, et al., 2012).

Several studies on confined ionospheric equatorial electrojet (EEJ) current which flows eastward at the dip equator on the dayside, and the occasional daytime reversal of EEJ current during quiet conditions often known as the counter electrojet (CEJ) current had been studied (Doumouya et al., 2003; Pedatella et al., 2011; Stening et al., 1996; Yamazaki et al., 2011). Basically, the interplay of the neutral winds, diurnal, and semidiurnal tidal oscillations in the upper atmosphere induced westward reversal of the EEJ strength on quiet days (Stening et al., 1996; Zhou et al., 2018).

Recent studies of the equatorial and low- and middle-latitude ionosphere have revealed strong longitudinal variations in EEJ strength, CEJ current, $E \times B$ drifts, and the ionospheric current system (e.g., Manoj et al., 2006; Maute et al., 2012; Soares et al., 2018). The longitudinal variability in the equatorial and low- and middle-latitude ionosphere is linked with the variability in the daytime ionospheric wind dynamo. Several studies have indicated that the interactions between the atmospheric tides, gravity, and planetary waves are the most likely source of longitudinal differences in the *E* region ionosphere (Bolaji et al., 2016; Fejer et al., 2010; Yamazaki, Yumoto, et al., 2012). In addition, the electrodynamic effects of South Atlantic Magnetic Anomaly, where the anomalous magnetic main field is weak and magnetic declination angle is large as compared to the rest of the regions, could also contribute to the longitudinal variations in the ionospheric *E* region (Abdu et al., 2005; Soares et al., 2018).

Many investigations had revealed that the upper atmosphere could be modulated by various electrodynamic coupling processes ranging from the quiet time (Rishbeth & Mendillo, 2001; Vineeth et al., 2007) to disturbed and geomagnetic periods (Richmond & Lu, 2000). Apart from the electrodynamical coupling between the *E* and *F* regions of the ionosphere during the quiet, disturbed, and geomagnetic storms periods, spectacular sudden stratospheric warmings (SSWs) were uncovered to modulate atmosphere and vertically couple the lower with the upper atmosphere via the middle atmosphere (Liu & Roble, 2002; Pedatella et al., 2018). When this dramatic meteorological phenomenon, which is due to dynamical forcing from the troposphere (Andrews et al., 1987; Charlton & Polvani, 2007), begins, abrupt increase in stratospheric temperature (ST) and deceleration of the stratospheric zonal mean zonal wind are significant. The prominent consequences were noticed in the ionospheric current systems (Bolaji et al., 2016; Yamazaki, Richmond, et al., 2012; Yamazaki, Yumoto, et al., 2012), CEJ currents (Vineeth et al., 2009), equatorial vertical upward $E \times B$ drifts (Chau et al., 2010; Fejer et al., 2010; Maute et al., 2015), ionospheric *F* region parameters (Patra et al., 2014; Pedatella et al., 2016), and total electron content (Chau et al., 2010; Goncharenko et al., 2010; Goncharenko et al., 2010; Pedatella & Forbes, 2010).

In recent years, the planetary wave activity in the mesosphere has received great attention, which unraveled a good deal of evidence about its nonlinear interaction with tides (Beard et al., 1999; Hagan & Roble, 2001; Liu & Roble, 2002; Maute et al., 2014; Mitchell et al., 1999; Pedatella & Forbes, 2010; Sridharan et al., 2002). Since the mesosphere/lower thermosphere region of the atmosphere is a potential medium that coupled the lower atmosphere to the ionosphere, the modulated local tides can influence ionospheric variability through the *E* region wind dynamo process at around 115 km (Abdu et al., 2006; Forbes et al., 2008; Maute et al., 2012). These interactions that can occur during the prevailing SSW conditions play a significant role in controlling the electrodynamics of ionospheric current system. For example, CEJ events are strongly associated with amplification of a lunar tidal component in the lower thermosphere (Fejer et al., 2010; Stening, 1989; Yamazaki, Yumoto, et al., 2012). This is attributed to changes in ST and zonal mean zonal wind during the SSW events (Stening et al., 1996; Bolaji et al., 2016) that modified the nonlinear interaction between planetary waves and tidal components (Vineeth et al., 2007, 2012).

Siddiqui et al. (2018), who focused on the SSW effects on the EEJ strength over the American sector, showed that the relative enhancement of the semidiurnal lunar amplitude in EEJ strength is observed to be higher than that of the solar semidiurnal amplitude in EEJ strength during the SSW events. Sathishkumar and Sridharan (2013) also revealed higher solar tidal variability that was compared to lunar tidal components in EEJ strength at the Asian sector. Evidence of varying tidal components in EEJ strength over the African sector during an SSW event is still primitive. The only exception is the study of Bolaji et al. (2016) who examined the effect of SSW on daily magnetic variation over Africa. To this end, the tidal characteristics during the SSW are explored and compared with the existing results in other longitudinal sectors.

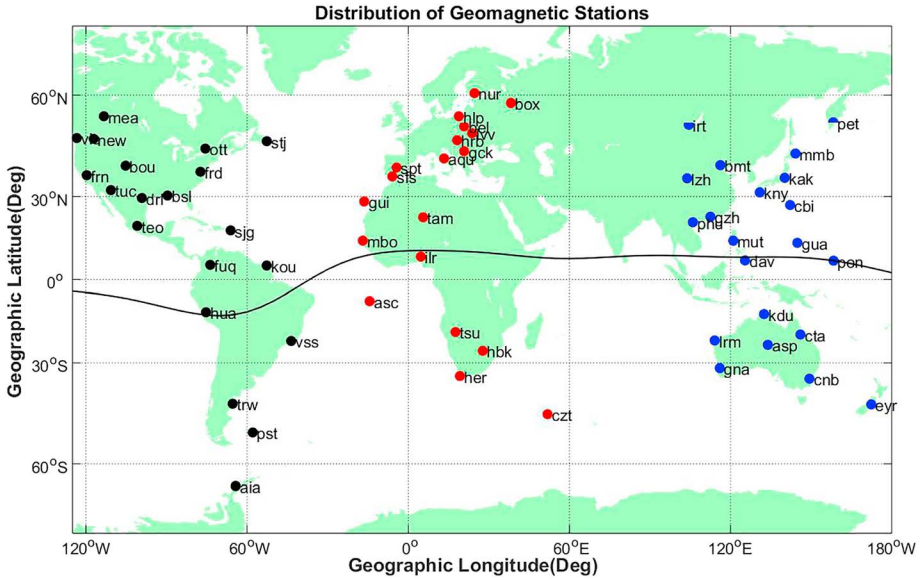

Figure 1. Distribution of the geomagnetic observatories and their abbreviation names used in the present study. The black line indicates the geomagnetic dip equator. The black, red, and blue dots symbolize geomagnetic observatories over the American, European-African, and East Asia-Australian sectors, respectively.

In this paper, we investigate the tidal components in EEJ strength that is responsible for significant reduction and enhancement in EEJ strength during the SSW event. Subsequently, the simultaneous connection between the ionospheric currents at the middle latitudes and the equatorial region current during the SSW event is examined. We specifically investigate two major SSW events (2005/2006 and 2008/2009) at three different longitudinal sectors, that is, American, East Asian-Australian, and European-African. We also compare our results with previous studies to improve our knowledge about key drivers of the ionospheric electrodynamics during the SSW event.

2. Data and Method of Analysis

In this study, we utilize the orthogonal magnetic field data obtained from several geomagnetic observatories networks. These include the International Real-time Magnetic Observatory Network (INTERMAGNET; Kerridge, 2001); World Data Centre for Geomagnetism (WDC), Edinburgh; Magnetic Data Acquisition System/Circum-pan Pacific Magnetometer Network (MAGDAS/CPMN; Yumoto & the MAGDAS Group, 2006); Ocean Hemisphere Network Project (OHP; Toh et al., 2006); and Japan Meteorological Agency (JMA). We considered the geomagnetic observatories covering both the Northern and Southern Hemispheres over the American, East Asian-Australian, and European-African sectors. In order to isolate the disturbances of polar jet currents produced by solar wind-magnetosphere dynamo processes, the observatories are restricted to ±60° quasi-geomagnetic latitudes (Weimer, 2013). The quasi-geomagnetic coordinates of these observatories were computed using the main field model (International Geomagnetic Reference Field, IGRF-2012 version) at the epoch of 2015-0 (Emmert et al., 2010) provided by the International Association of Geomagnetism and Aeronomy (IAGA) with their geographic distribution shown in the map of Figure 1.

The lower stratospheric parameters comprising zonal mean zonal wind (60°N) and ST (90°N) at 10 hPa (~32-km altitude) were obtained from the National Centers for Environmental Prediction-National Center for Atmospheric Research (NCEP-NCAR) (https://www.esrl.noaa.gov/psd/), to study the influence of meteorological forcing on different current systems in the ionosphere. Further details regarding the NCEP-NCAR reanalysis data can be found in Kalnay et al. (1996). In order to investigate the impact of planetary wave activity on EEJ strength, we obtained the planetary waves with zonal wave number 1 (Z1) and zonal wave number 2 (Z2) in geopotential height at 10 hPa and 60°N from the NASA database (http://acdbext.gsfc.nasa.gov/Data_services/met/ann_data.html) during both SSW events.

Next, we converted the geomagnetic field data reported in orthogonal geographic coordinates (northward, X, and eastward, Y, geographic components) to orthogonal geomagnetic components (horizontal intensity, H, and declination, D) using routine procedure prior to further processing. The D in degrees was converted to their equivalent geomagnetic eastward variation field strength in nanotesla (nT). The choice of converting the X and Y to H and D components were the uniformity in the field components of the several magnetometer arrays considered.

In order to compute the daily geomagnetic field variation, we first convert the 1-min resolution of H, D, and Z orthogonal field components to hourly values. Further data processing procedures were involved in the analysis, which synoptically entails elimination of unusual spikes and linear interpolations, baseline removal, midnight departure adjustment, and disturbance storm time (*Dst*) corrections (Love & Gannon, 2009; Takeda & Araki, 1984). Thus, the *Sq* variations labeled ΔH, ΔD, and ΔZ were derived based on local time concept and simultaneously subjected to spherical harmonic analysis (SHA), and both the external and internal equivalent ionospheric current functions were derived accordingly. Further details regarding the SHA can be found in the following studies: Matsushita and Xu (1984), Campbell et al. (1993), and Yamazaki et al. (2011). In this study, the maximum index of the spherical harmonic expansion chosen is 4 in order to exclude grosser errors caused by higher harmonic terms and resolve the large-scale structure of the current system (Takeda, 1999). In SHA, the geomagnetic observatories within ±3° quasi-geomagnetic latitude on each side of the magnetic equator are omitted in order to prevent the potential disturbances of equatorial jet current system. In this study, the external portion of this current flowing in a thin conducting spherical shell at 110-km altitude was investigated in relation to both SSW events.

Prior to SHA, the time-dependent hourly ΔH data situated at the EEJ footprint and outside the EEJ band (Yacob, 1977) were obtained to derive the EEJ current strength. For this purpose, ΔH data at Huancayo (HUA: 0.32°S, 2.55°W) minus ΔH data at Fuquene (FUQ: 16.16°N, 0.63°W) were considered to characterize the EEJ current over the dip equator in the American sector. We used ΔH data at Davao (DAV: 0.3°S, 197.82°E) minus ΔH data at Muntinlupa (MUT: 7.58°N, 193.58°E) to compute the EEJ current strength for the Asian sector during the 2005/2006 SSW event. We used magnetic data of Ponape (PON: 0.63°N, 230.43°E) minus ΔH data at Guam (GUA: 06.12°N, 216.99°E) for the 2008/2009 event. Similar computation is applied to ΔH data at Mbour (MBO: 3.42°N, 57.96°W) minus ΔH data at Ascension Island (ASC: 19.59°S, 56.13°W) and ΔH data at Ilorin (ILR: 3.62°N, 79.34°E) minus ΔH data at Tamanrasset (TAM: 12.82°N, 80.30°E) during the 2005/2006 and 2008/2009 SSW events, respectively. Both stations considered in each sector have similar quasi-geomagnetic longitudes. Thereafter, the afternoon CEJ events (hereafter referred to as CEJ) for each sector were selected by taking the magnitude of the minimum hourly values of EEJ current in the interval 14–18 hr local time (LT) and averaging it for each day (Pandey et al., 2018; Soares et al., 2018). We also noted frequent CEJ occurrence in the morning sector from 6 to 10 LT and an occasional noon CEJ that happened for a few hours in the local noon sector. Such investigations of morning CEJ and noon CEJ occurrences are, however, beyond the scope of this paper.

In order to extract the dominant tidal variations in the EEJ current system during the SSW, the derived EEJ current is decomposed to compute corresponding amplitude and Fourier phasing of the harmonics up to selected harmonic ranks that are determined by the least squares method. Decomposition starts by dividing each cycle of each data into 24 equal width strips at an interval of 15°. The mathematical representation is as in equation (1).

$$S = \sum_n s_n \sin(nt + \gamma_n) = \sum_n A_n \cos nt + B_n \sin nt \quad (1)$$

where $A_n = s_n \sin \gamma_n$ and $B_n = s_n \cos \gamma_n$ are the solar harmonic coefficients. At $n = 0$ yields the time-dependent zonal average of the series. Here s_n and γ_n are the solar amplitude and phase associated with the nth harmonic component, respectively, and t represents the solar time (or LT) in hour. The first three harmonic components (with periods 24, 12, and 8 hr) in amplitude (nT) and phase (hr) were computed and studied in relation to both SSW events.

Similarly, the lunar harmonics function of EEJ current is computed by using the Chapman-Miller approach (Chapman & Bartels, 1940). The dominant lunar daily variation is the semidiurnal term (those for which $n = 2$) that has a period half of lunar day (with period =~12.42 hr) as shown in equation (2). Recent approaches

to determine the amplitude and phase of lunar tides in geophysical data using Chapman's phase law are discussed in Yamazaki and Maute (2016) and Siddiqui et al. (2018). The mathematical representation of the lunar daily variations of a geophysical parameter can be expressed as in equation (2).

$$L = \sum_n l_n \sin(n\tau + \phi_n) = \sum_n a_n \cos n\tau + b_n \sin n\tau \quad (2)$$

The lunar harmonic coefficients are given as $a_n = l_n \sin \phi_n$ and $b_n = l_n \cos \phi_n$. Here l_n is the amplitude of lunar harmonic and ϕ_n is the phase of lunar harmonic component. The mean lunar time in hours is given by $\tau = t - \nu$, where ν indicates the phase of the Moon (lunar age), which increases from 0 hr at the mean new moon to 24 hr during each synodic lunation. The lunar age ν is thus determined for each day according to $\nu = \lambda_M - \lambda_S$, where λ_M and λ_S symbolize the mean longitudes of the Moon and Sun, respectively, calculated from equations (3) and (4) below:

$$\lambda_M = 283.612983° + 13.176396730246° t_d + 0.00198° T^2 \quad (3)$$

$$\lambda_S = 280.682325° + 0.985647335387° t_d + 0.00030° T^2 \quad (4)$$

where t_d is the number of days that have elapsed since 12 hr Greenwich mean time on 1 January 1900 and where T is the same time measured in the Julian century of 36,525 solar days as unit (Sugiura & Fanselau, 1966).

We obtained the solar and semidiurnal lunar tidal components simultaneously based on a 21-day running window at a 1-hr step over the entire period of the SSW events. The application of 21-day running mean of the EEJ current makes possible a more reasonable estimation of the solar and lunar tides of the EEJ current (Chau et al., 2015; Siddiqui et al., 2018).

3. Observational Results

The ST profile at 90°N and zonal mean zonal wind (U) at 60°N over 10-hPa pressure level are shown in Figures 2a and 2b during the 2005/2006 and 2008/2009 SSW events, respectively. These daily ST and U data are obtained from NCEP-NCAR reanalysis between December 2005 and March 2006, on one hand, and between December 2008 and March 2009, on the other hand. During the 2005/2006 SSW event, two minor warming episodes were recorded in early January (no evident reversal of U), which was followed by a major SSW peaked around day 53 after U started reversing around day 51 (Figure 2a). In contrast, it is clearly seen that the ST shows one peak and professed no other drastic variation during the 2008/2009 SSW event. The reversal of U is evident in late January, revealing that there was a major warming. Both polar stratospheric warming events were registered as the strongest and prolonged events having the maximum temperature peak accompanied by marked variation of U with a couple of days lag (Manney et al., 2008).

The planetary wave activity with zonal wave numbers (Z1 and Z2) during the same periods is also shown in Figures 2c and 2d. Before the first 2005/2006 minor SSW (when the ST reaches its peak around day 35) and U commences deceleration around day 33 (Figure 2a), Z1 had maximized on day 1 (~1,050 m) and around day 17 (~1,124 m). In the case of the 2008/2009 SSW event, before Z2 peaks on day 51 (~1,150 m), Z1 had reached its peak on days 4 (~1,340 m) and 15 (~1,328 m). Z1 reaches another maximum value (~1,328 m) ~21 days later (around day 38, Figure 2c). This was when the ST of the second minor SSW was attempting to reach its peak and coincided with a period when U was decelerating. The shaded region in gray color in Figures 2a and 2c that begins from 1 January 2006 and ends 2 March 2006 indicates the period of the SSW event. For the 2008/2009 SSW event, it begins 17 January 2009 and ends 10 March 2009 (Figures 2b and 2d).

In addition, the geomagnetic conditions during both events are shown in Figures 2e and 2f. During both events, the average solar radio fluxes were found to be 80 and 68 sfu, respectively, indicating low solar activity condition. The Kp index ranges from 0 to 6 units with a mean of 5 units. This suggests that the magnetosphere-ionosphere coupling process was moderate during both events. The black dashed lines in all the figures in this study represent the decelerating climax of U at 10 hPa, and the shaded gray color in the remaining plots is the period of the events.

Figure 3 shows the contour plots of EEJ strength over the American, Asian, and African sectors with the superimposed open and solid circles, which indicate the phases of full and new moon periods,

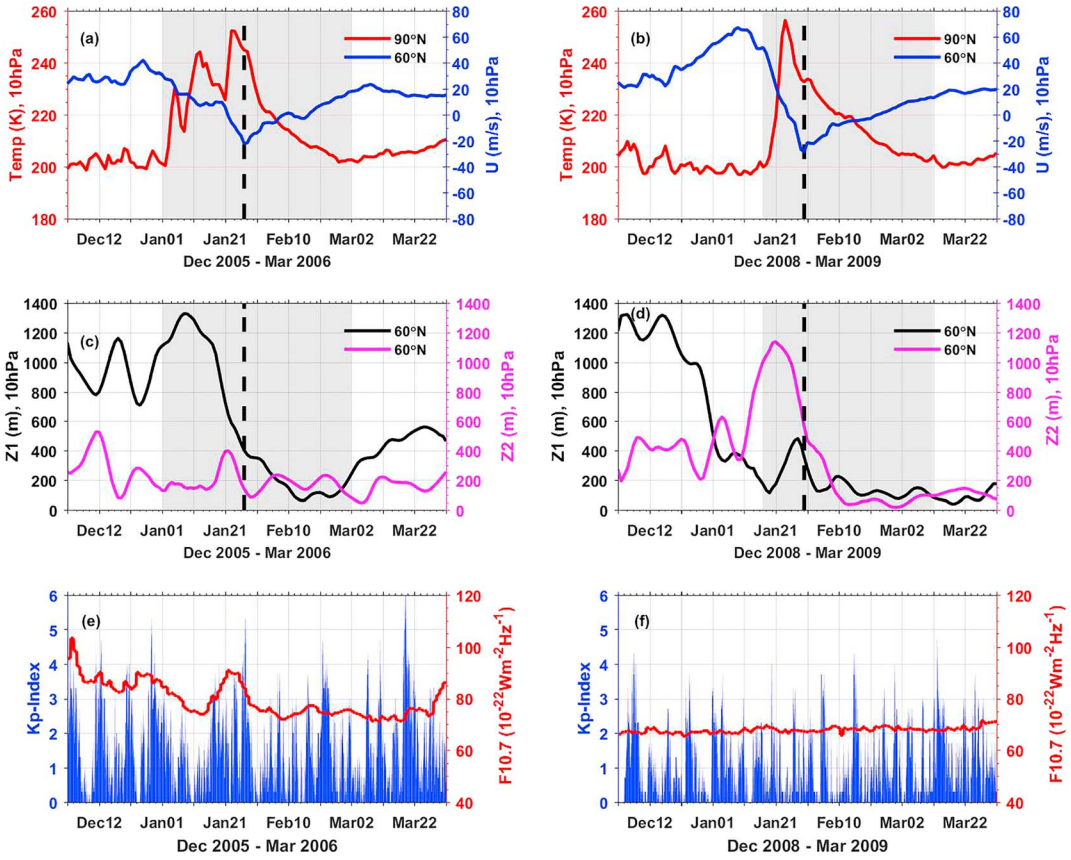

Figure 2. (a) The stratospheric temperature (red line) at 90°N and zonal mean zonal wind (*U*, blue line) at 60°N and 10 hPa derived from the National Centers for Environmental Prediction-National Center for Atmospheric Research data set during the 2005/2006 sudden stratospheric warming (SSW) event. (b) The same as (a) but for the 2008/2009 SSW event. (c) The planetary wave activity with zonal wave number 1 (Z1, black line) and zonal wave number 2 (Z2, magenta line) of the geopotential height at 60°N and 10 hPa. (d) The same as (c) but for the 2008/2009 SSW event. The shaded portion in gray is the duration of the events. The periods of the maximum SSW event is marked by vertical black dashed lines. The corresponding geospace conditions are shown in (e) and (f), respectively. The daily $F_{10.7}$ solar radio flux is depicted in the right vertical scale units by the red solid line. The *Kp* index is given by the blue shaded area.

respectively, during both SSW events. The EEJ strength shows strong longitudinal differences. It will be seen that the magnitude of the EEJ strength in the American sector is large, confirming the orthogonality effects of geomagnetic main field and dip equator. The magnetic field anomaly in the Asian and African ionosphere is almost horizontal, thereby showing least variability in EEJ strength as compared to that of the American sector. This large magnitude in magnetic field strength brings about strong EEJ, CEJ, and ionospheric current system in the American sector. The longitudinal variability of the EEJ strength could also be attributed to changes in the lower atmosphere during an SSW event.

It is clearly observed that there is a significant enhancement in EEJ strength seen in the East Asian and African sectors during the 2005/2006 minor SSW between days 32 and 37 (Figures 3c and 3e) that was absent in the American sector (Figure 3a). Figure 4 illustrates the CEJ strength over the American, Asian, and African sectors during the 2005/2006 and 2008/2009 SSW events. Superimposed on these figures are the ST, *U*, Z1, and Z2 activities during both SSW events. It is clearly seen that more CEJ occurrences are obvious during the SSW-induced period compared to the precondition period. Around days 41–46, when the decelerating *U* is about reversing, significant CEJ current followed by enhancement in EEJ current occurred in the American sector during the 2006 SSW event (Figure 4a). Instead of significant CEJ current seen in the American sector, we observed significant reduction in EEJ strength in the East Asian sector (Figure 3c) around days 41–46. In the African sector around days 41–46, the evolving CEJ event that started during the precondition period became invisible (Figure 4e). These significant CEJs in the American sector, reductions in EEJ strength in the East Asian sector, and reductions in CEJs in the African sector seen around days 41–46 were obviously near the full moon periods. Just after the reversing *U* peaks around day 57, both Z1 and

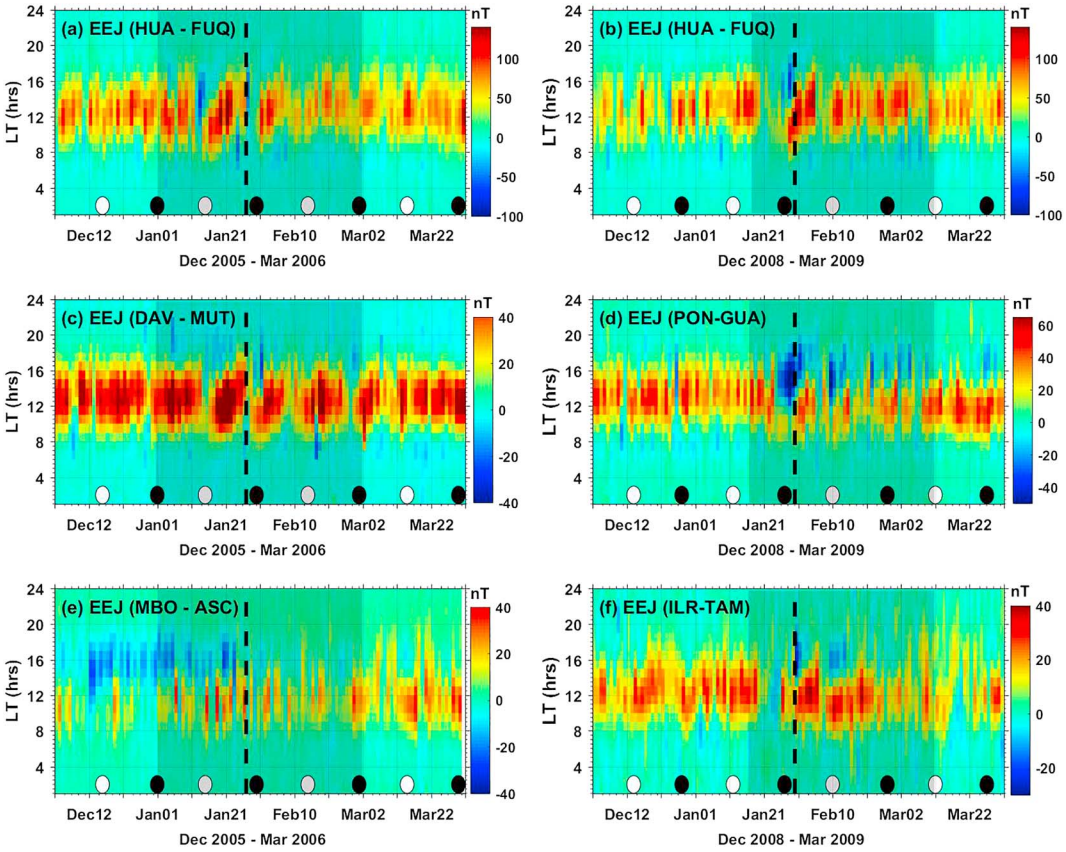

Figure 3. Daily variation of equatorial electrojet (EEJ) strength at the (top) American, (middle) East Asian-Australian, and (bottom) European-African sectors during the (left) 2005/2006 and (right) 2008/2009 sudden stratospheric warming events. The phases of full and new moon periods are indicated by the open and solid circles, respectively. The shaded portion in gray is the duration of the events and the periods of the maximum sudden stratospheric warming event is marked by vertical black dashed lines. LT = local time.

Z2 had subsided below 400 m around day 59. The immediate consequence seen in all of the stations just after the reversing *U* had reached its peak was a significant reduction in EEJ strength (Figure 3a). A CEJ occurrence began 2 days later (day 53) after the peak in Z2 and decreasing EEJ current strength over the American, East Asia, and African sectors on day 51. This is a period when the ST was attempting its peak and *U* was decelerating. Around day 58 (Figure 2d), which coincided with the maximum reversal in *U*, a significant CEJ current occurred over the American (Figure 4b) and East Asian (Figure 4d) sectors. A similar CEJ current feature found in the African sector (Figure 4f) was moderate. Around day 67 when the peak reversal of *U* was accelerating, both Z1 and Z2 had subsided below 400 m. The immediate consequence, which was obvious in all of the stations, is a significant reduction in EEJ strength (Figures 3b–3d). A feature that persists until day 71 in the American sector was absent in the East Asian and African sectors. The changes seen over the next couple of days in the East Asian and African ionosphere were moderate CEJ currents associated with varying EEJ strength. All of these CEJ occurrence events in the American, East Asian, and African sectors during the 2008/2009 SSW appeared near the new moon and full moon periods.

Figure 5 shows the solar and lunar semidiurnal tidal variabilities during the 2005/2006 and 2008/2009 SSW events over the American, Asian, and African sectors. It is evident that the tidal variability is enhanced during both events. Figure 6 shows the diurnal and terdiurnal amplitude variabilities in EEJ strength for the same periods. It is important to note that EEJ strength is due to tidal wind-driven dynamo on a global scale (Forbes, 1981). One can understand that while the observed *U* was decelerating during the 2005/2006 SSW event, the increasing solar semidiurnal tidal amplitude in EEJ strength that started increasing around day 41 maximized in the American (Figure 5a) and East Asian sectors (Figure 5c). However, similar interactions involving solar semidiurnal and increasing lunar semidiurnal tidal amplitude in EEJ strength that occurred closer to the peak of the reversing *U* around days 41–46 were observed during the 2008/2009 SSW event

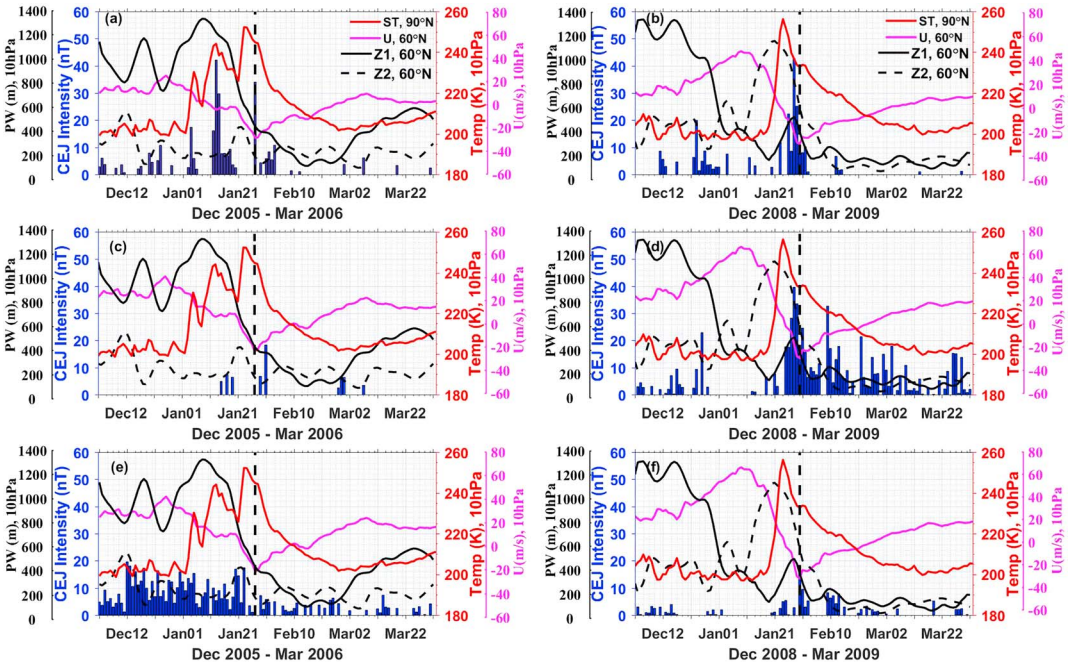

Figure 4. The occurrence frequency of afternoon counter electrojet (CEJ) intensity at the (top) American, (middle) East Asian-Australian, and (bottom) European-African sectors during the (left) 2005/2006 and (right) 2008/2009 SSW events. The periods of the maximum sudden stratospheric warming event is marked by vertical black dashed lines. Comparison of the daily variation of stratospheric temperature (ST, red line) at 90°N and 10 hPa, the zonal mean zonal wind (*U*, magenta line) at 60°N and 10 hPa, the planetary wave (PW) activity with zonal wave number 1 (Z1, black line) and zonal wave number 2 (Z2, dashed black line) of the geopotential height at 60°N and 10 hPa.

(Figure 5b). The lunar semidiurnal tidal amplitude is a little larger than the solar semidiurnal amplitudes before the onset of the SSW. The interactions between both tides during both SSW events modulated EEJ strength in all of the sectors and initiated significant CEJ current associated with significant enhancement in EEJ strength. Over the Asian and African sectors, the solar and lunar semidiurnal tidal amplitudes are comparable, a result that is in accordance with the results of Sathishkumar and Sridharan (2013) and Siddiqui et al. (2018). The diurnal amplitude in EEJ strength at any sector is larger during both SSW events (Figures 6a and 6b). During both SSW events, the terdiurnal magnitude over the African sector is small (~2 nT) as compared to that in the Asian sector (~4 nT) and the American sector (~7 nT). While the diurnal tides over the African sector is comparable to that of the Asian sector during the 2008/2009 SSW event, it is significantly higher at the African sector around day 71.These features observed in the American and Asian sectors are consistent with the previous study (e.g., Sathishkumar & Sridharan, 2013). To further understand the tidal variability in EEJ strength, the solar and lunar semidiurnal phases in EEJ strength at different sectors during both SSW events are shown in Figures 7 and 8, respectively. It is clearly seen that the solar semidiurnal phases recorded a steady increase before the SSW and peak during the onset of the SSW in the American, Asian, and African sectors during the 2008/2009 SSW event (Figures 7b, 7d, and 7f). During the SSW onset, there is a decline in the tidal phases from 12.5- to 11.2-hr, 13- to 10.5-hr, and 12.5- to 11-hr solar LT over the American, Asian, and African sectors, respectively. Thereafter, the long-lasting SSW effects hinder the solar tidal phases to return to its SSW precondition position after the warming. In contrast, during the 2005/2006 SSW event, the solar phase variability in EEJ strength over the American sector remains constant at about 11.5-hr solar LT before the onset of the SSW event (Figure 7a). During the SSW onset, it decreases to about 10.5-hr solar LT. Over the Asian sector, the solar phase variabilities in EEJ strength became downward at about 12 hr and were consistent (Figure 7c). This is different from the solar phase variability observed in the African sector, which increased at about 9 hr and did not change appreciably during the entire period of the SSW event (Figure 7e). These typical tidal variabilities that were obvious near the new or full moon periods revealed the influence of tidal oscillation in EEJ current during the SSW events as previously reported by Fejer et al. (2010). During this period, the lunar semidiurnal phase oscillation does not change noticeably

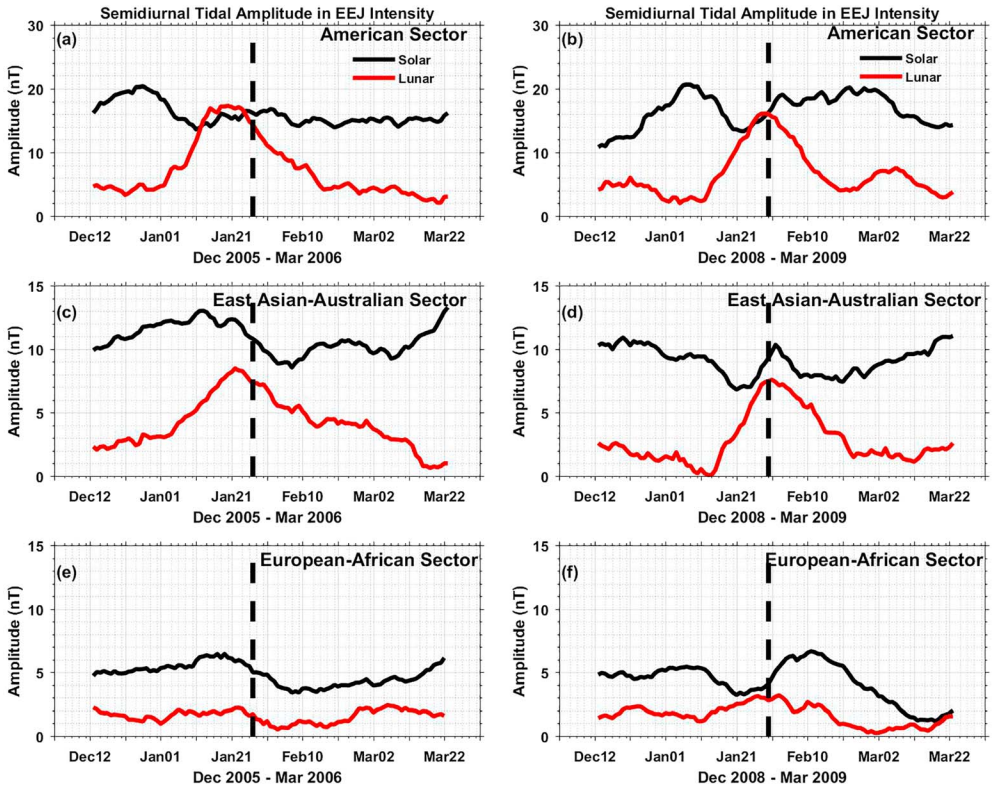

Figure 5. Solar and lunar semidiurnal components in the equatorial electrojet (EEJ) strength at the (top) American, (middle) East Asian-Australian, and (bottom) European-African sectors during the (left) 2005/2006 and (right) 2008/2009 sudden stratospheric warming events. The black and red lines represent the solar and lunar semidiurnal tidal amplitudes of EEJ strength, respectively. The periods of the maximum sudden stratospheric warming event is marked by vertical black dashed lines.

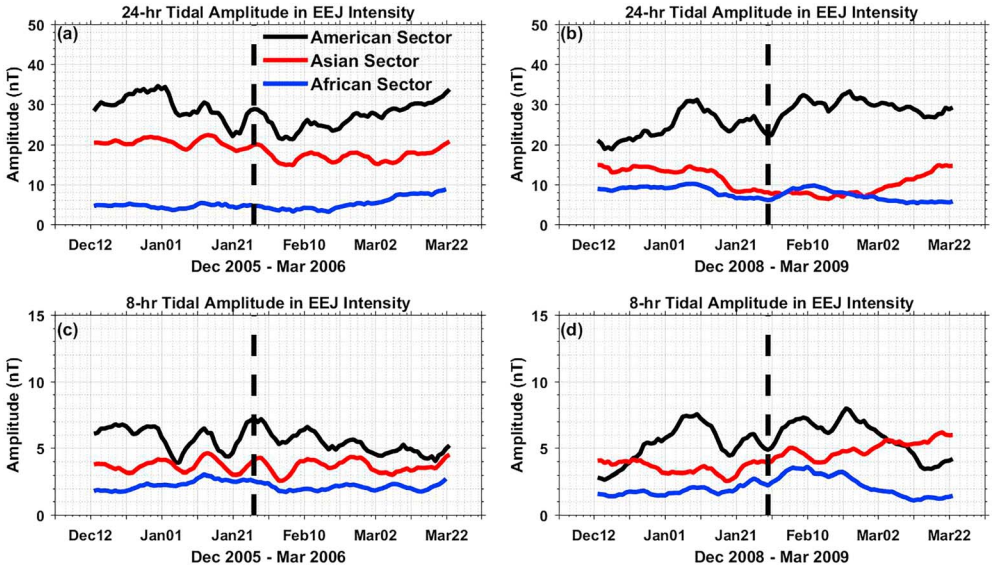

Figure 6. Solar diurnal (24-hr) and terdiurnal (8-hr) components in equatorial electrojet (EEJ) strength during the (left) 2005/2006 and (right) 2008/2009 sudden stratospheric warming events, respectively. The black, red, and blue lines represent the tidal amplitude of EEJ strength at the American, Asian, and African sectors, respectively. The periods of the maximum sudden stratospheric warming event is marked by vertical black dashed lines.

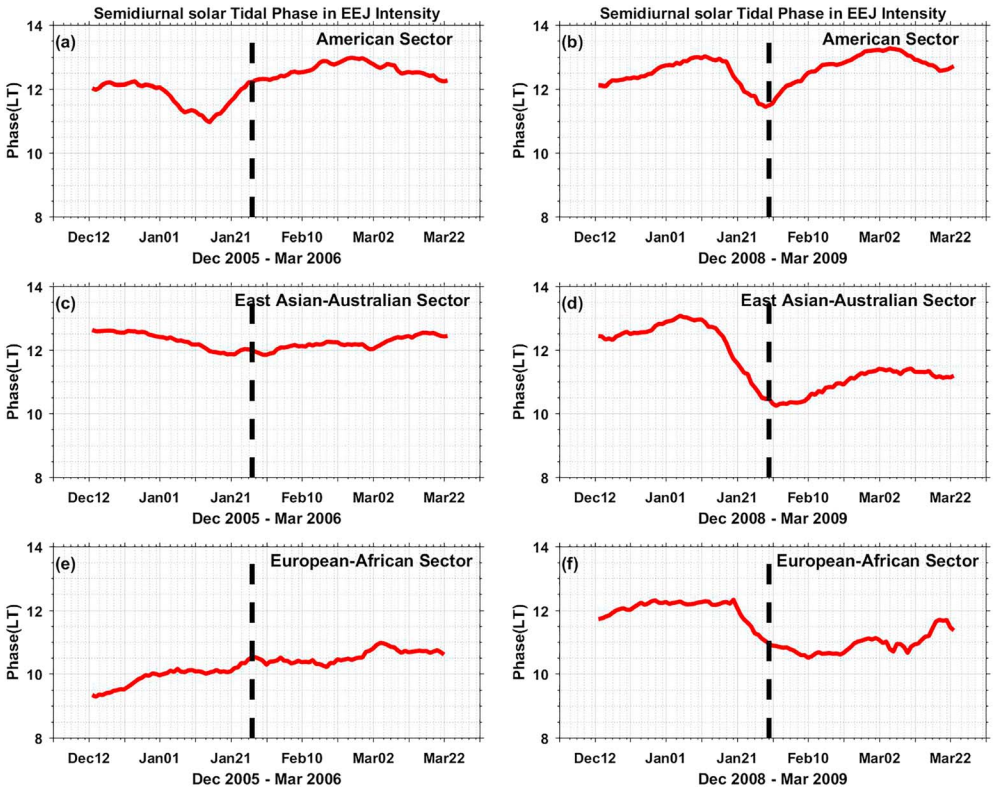

Figure 7. Solar semidiurnal tidal phases in equatorial electrojet (EEJ) current at the (top) American, (middle) East Asian-Australian, and (bottom) European-African sectors during the (left) 2005/2006 and (right) 2008/2009 sudden stratospheric warming events. The periods of the maximum sudden stratospheric warming event is marked by vertical black dashed lines. LT = local time.

except in the Asian and African sectors where the lunar semidiurnal phase is slightly perturbed before and after the SSW event, respectively (Figures 8d and 8f). The perturbations involved are moderate and consistent with the earlier studies and revealed here with little differences in phase shift (Sathishkumar & Sridharan, 2013; Siddiqui et al., 2018).

The distribution of an equivalent ionospheric current system shown in Figures 9 and 10 was obtained by SHA during the 2005/2006 and 2008/2009 SSW events, respectively. A CEJ associated with significant increase in EEJ strength over the American sector during the 2005/2006 SSW responded to a brief increase in ionospheric current (Figure 9c) that was immediately followed by a brief reduction at a southern middle-latitude station (PST). Surprisingly, there are no significant changes in the equivalent ionospheric current (Figure 9a) due to SSW at a northern middle-latitude station (FRN). However, a significant reduction in ionospheric current (Figure 9b) was obvious after U reverses during the 2006 SSW at a low-latitude station in the Northern Hemisphere (KOU). All of these scenarios seen in the American sector at a different station during the 2005/2006 SSW (Figures 9a–9c) were repeated in the East Asian-Australian (Figures 9d–9f) and European-African (Figures 9g–9i) sectors. These results seen at different stations at different longitudes during the 2005/2006 SSW were repeated in the 2008/2009 SSW event. The results presented here noticeably revealed the longitudinal differences in EEJ current and the ionospheric current system.

4. Discussion

Our results have shown that the solar and lunar tidal components in EEJ strength, CEJ current, and ionospheric current exhibit strong longitudinal variations. We found that a significant CEJ current associated with EEJ strength occurred in the American sector (Figure 3a) when the decelerating U is about reversing during the 2005/2006 SSW event. In comparison to the well-investigated 2008/2009 SSW event (Bolaji et al., 2016; Vineeth et al., 2007; Yamazaki, Yumoto, et al., 2012), similar feature appeared in the

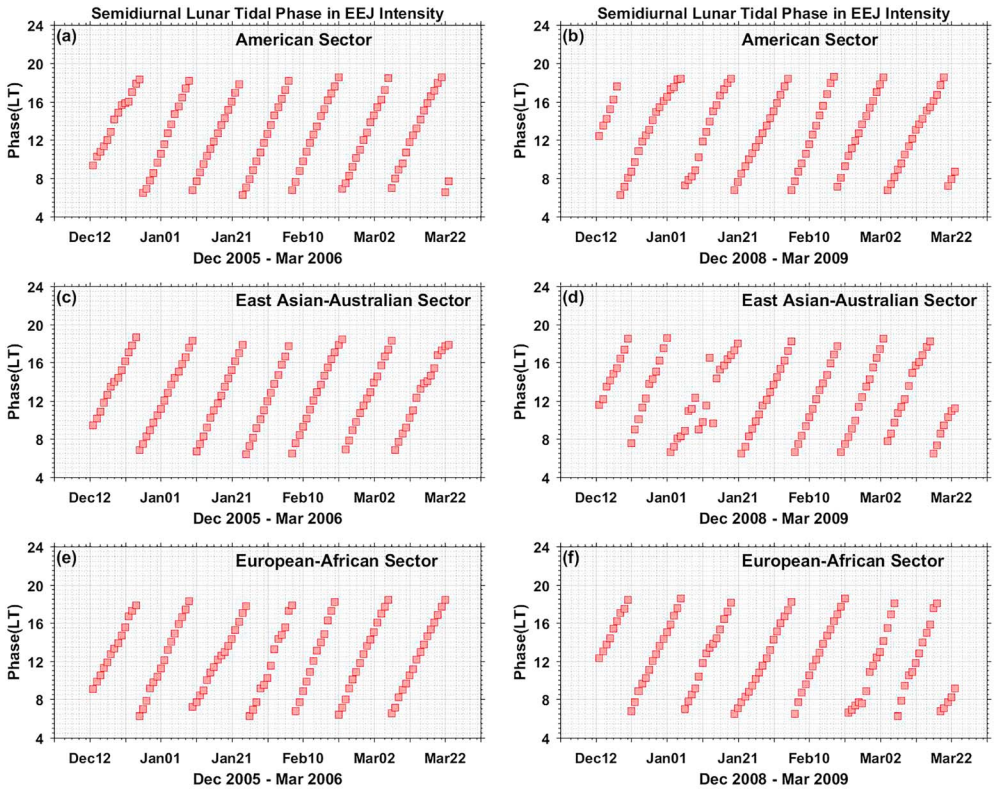

Figure 8. Same as Figure 7 but for lunar semidiurnal tidal phases.

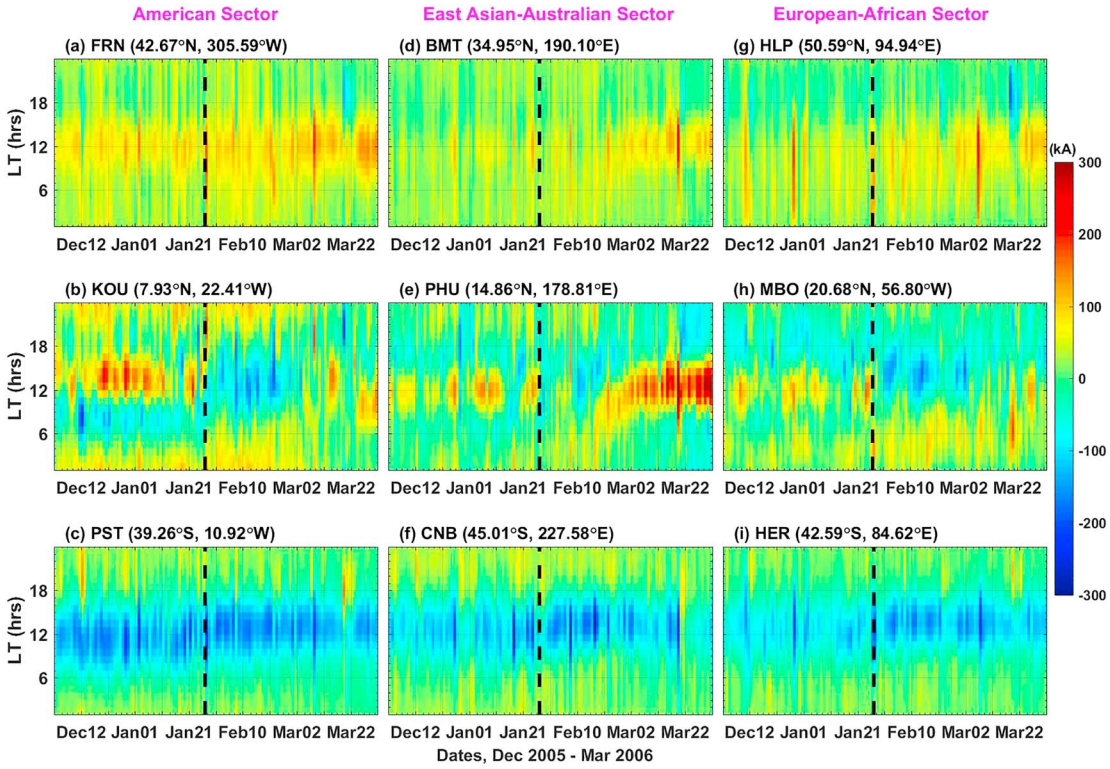

Figure 9. Equivalent ionospheric current over the low and middle latitudes at the (a–c) American sector, (d–f) East Asian-Australian sector, and (g–i) European-African sector during the 2005/2006 sudden stratospheric warming event. The periods of the maximum sudden stratospheric warming event is marked by vertical black dashed lines.

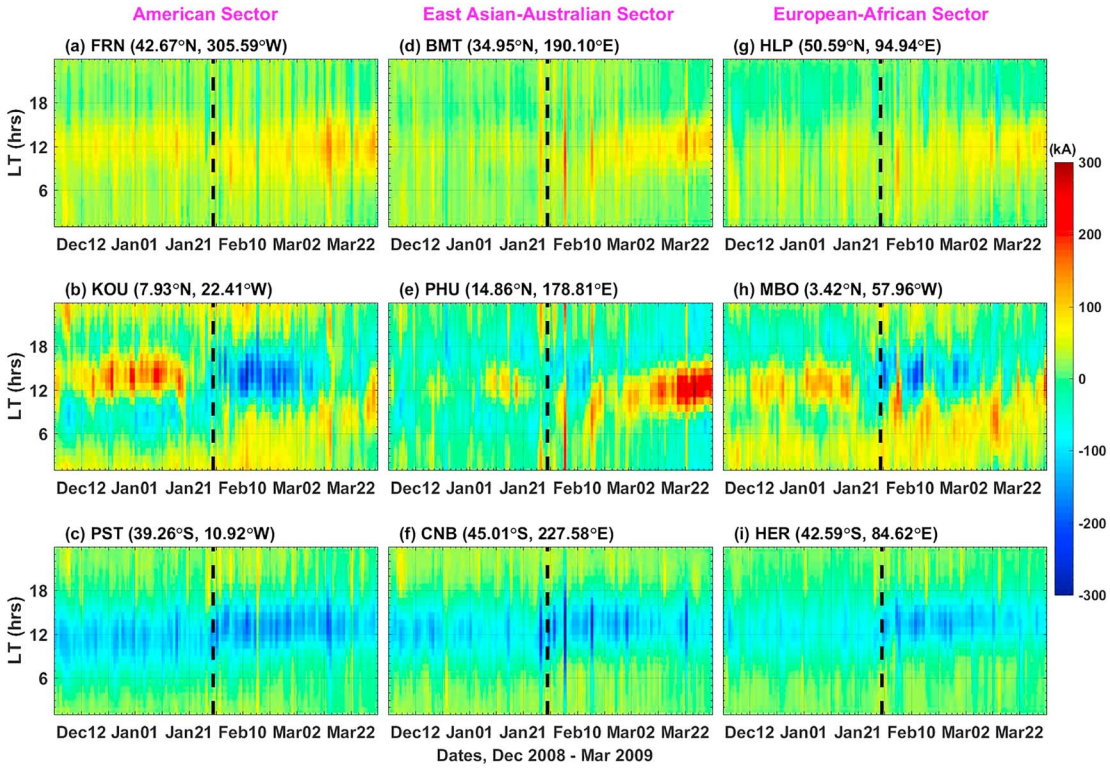

Figure 10. Same as Figure 9 but for the 2008/2009 sudden stratospheric warming event.

American sector when the reversing *U* is around its maximum (Figure 3b). This surprising disparity in timing and signature of the varying *U* between the 2005/2006 and 2008/2009 SSW events further doubt *U* as the major facilitator of a significant CEJ current. Despite this, the role of the varying *U* cannot be ignored because it can modulate EEJ strength (Siddiqui et al., 2018). During both SSW events, a significant CEJ became obvious just after Z1 had reached its maximum while Z2 was increasing (Figures 4a and 4b). These are periods around the peak of Z1 and Z2 as evident in the 2005/2006 (Figure 2c) and 2008/2009 (Figure 2d) SSW events and indicate that a strongly enhanced Z1 and Z2 activities were evolving. Apart from these cases of strongly enhanced Z1 and Z2 activities (when varying Z1 and Z2 are both increasing) seen during the SSW-induced periods, cases of moderately enhanced (when varying Z1 is increasing and Z2 is decreasing, or vice versa) and weakened (when varying Z2 and Z1 are both decreasing) Z1 and Z2 activities were obvious during the 2005/2006 SSW precondition (between days 1 and 31) and after the 2008/2009 SSW event (between days 81 and 116), respectively.

It is very crucial to recall that strengthened planetary waves do not propagate by themselves to the upper atmosphere because they are restricted to the mesosphere/lower thermosphere of high- and middle-latitude regions (Pancheva et al., 2009; Pogoreltsev et al., 2007). A well-known mechanism supported by previous efforts (Liu et al., 2004; Liu & Roble, 2005), which explains how planetary waves originating in the lower atmosphere can propagate and impact the ionosphere, is the nonlinear interaction of planetary waves with tidal components (diurnal, semidiurnal, and terdiurnal) at lower altitudes (Charlton & Polvani, 2007; Hagan & Forbes, 2002). When strengthening planetary waves activity interact nonlinearly with tidal components, changes in the lower atmospheric circulation pattern are initiated (Hagan & Roble, 2001; Liu & Roble, 2002). These changes can facilitate easy upward propagation of planetary waves from stratospheric altitudes to lower thermospheric heights during an SSW event. These changes modified tidal amplitudes at the upper mesospheric altitudes of high-latitude coupled *E* region wind dynamo (Abdu et al., 2006; Forbes, 1981) and low-latitude ionosphere (Sathishkumar et al., 2009). As an example, strongly enhanced planetary waves interacting nonlinearly with varying tidal amplitudes in EEJ strength (Figure 5a) when *U* was decelerating during the 2005/2006 SSW event was seen around days 41–51. Around this period when a strongly enhanced Z1 and Z2 activity persists (10 days after Z1 had reached its maximum and when Z2 reaches its maximum),

an interesting increase of 24- (solar diurnal, Figure 6a) and 12-hr (lunar semidiurnal, Figure 5a) tidal amplitudes in EEJ strength was significant in the American sector. As can be observed from our results (Figure 6a), a solar diurnal signature was significantly higher than both lunar and solar semidiurnal tidal components in the American sector. In addition, a lunar semidiurnal signature was higher than a solar semidiurnal signature (Figure 5a). Before the lunar semidiurnal tidal component in EEJ strength reaches its maximum value during the 2005/2006 SSW-induced period around days 41–51, a solar semidiurnal that is higher than a lunar semidiurnal tidal component had reached its maximum value in the East Asian and African sectors.

An exception found in the American sector was a solar diurnal tidal component that peaked before other tidal components reach their peaks. Contrary to the American sector, the immediate effect of a solar semidiurnal tidal component in EEJ strength that peaked earlier before other tidal components reach their peaks around days 41 and 51 does not lead to a significant CEJ in the East Asian and African sectors. Instead, a significant reduction in EEJ strength and CEJ intensity is obvious in the East Asian and African sectors (Figures 3c and 3e), respectively. Other tidal components that are strongly associated with a reduction in EEJ strength (East Asia)/CEJ intensity (Africa) during those times are solar diurnal and terdiurnal components. Our results revealed that their values were actually increased at those times (Figure 5a). This is an indicator that they are partly associated with a reduction in EEJ strength over the East Asian sector and in CEJ intensity over the African sector. Although a solar diurnal component was significantly higher than a solar semidiurnal component, a solar semidiurnal component peaks before a solar diurnal component reaches its peak.

When *U* was reversing during the 2008/2009 SSW (Figure 2b), a lunar semidiurnal tidal component in the American and East Asian sectors had reached its maximum value, while other tidal components were varying (Figures 5b and 5d). We, therefore, suggest that these significant CEJ events that occurred when *U* was reversing were associated with lunar origin. Also, in the African sector (Figure 5f), a lunar semidiurnal tidal component that its maximum value earlier strongly accompanied CEJ events seen just after the reversing *U* had reached its peak (this varying African lunar tidal component was significantly lower compared to that of the American sector; Figure 5b). Similar significant amplification of a lunar semidiurnal tide linked to CEJ current during the SSW events are consistent with previous efforts of Stening et al. (1996), Fejer et al. (2010), and Sathishkumar and Sridharan (2013).

In addition to a lunar semidiurnal tidal component that reaches its maximum value earlier compared to other tidal components, a solar diurnal tidal component in a similar manner was strongly associated with a significant CEJ during the 2005/2006 SSW event in the American sector. This implies that CEJ occurrence during different SSW events at different longitudinal sectors is strongly related to different tidal components. Just after a significant CEJ in the American sector during both SSW events (Figures 3a and 3b), significant enhancements in EEJ strength were obvious. During the 2005/2006 SSW, similar significant enhancement in EEJ strength was seen at the East Asian sector after a significant reduction in EEJ strength (Figure 3c). We, therefore, suggest that in the American sector during the 2005/2006 SSW, significant enhancement in EEJ strength was accompanied by an enhancement of a lunar semidiurnal tidal component in EEJ strength. This is because while a solar diurnal tidal component associated with CEJ was reducing, a lunar semidiurnal tidal component reaches its peak value (Figure 5a). In addition, it is higher than that of a solar semidiurnal component (Figure 5a). However, significant enhancement in EEJ strength seen in the American sector during the 2008/2009 SSW and that of the East Asian sector during the 2005/2006 SSW were accompanied by a solar semidiurnal tidal component.

In the case of the American sector during the 2008/2009 SSW, this is obvious when *U* was reversing (Figure 2b) and a solar semidiurnal tidal component increases significantly (Figure 5b). It, later on, became higher than that of a lunar semidiurnal tidal component that was subsiding. We, therefore, conclude that enhancement of a lunar or solar semidiurnal tidal component that peaks before other tidal components reach their maximum values during an SSW can significantly enhance EEJ strength. Interestingly, most of these daily tidal components prior to and after both SSW events are high, moderate, and low in the American, East Asian, and African sectors, respectively. This can be one of the reasons why EEJ intensities in the American sector during both SSW events are significant compared to all of the EEJ intensities in the East Asian and African sectors when SSW events are not evolving. The South Atlantic Magnetic Anomaly

electrodynamics could contribute to this longitudinal variation in the EEJ strength over the American sector. An exception found between days 66 and 81, which can be linked to the CEJ events seen in the African sector around days 71 and 76, was a surge in the diurnal tidal component in EEJ strength. This surge that reached ~10 nT around days 71 and 76 over the African sector when the 2008/2009 SSW was subsiding was higher than that one over the East Asian sector (~8 nT). The physical mechanism responsible for this surprising scenario remained unknown and can be considered as a future research topic.

In the context of CEJ intensity, despite the fact that this diurnal tidal component in the African sector is higher when compared to that of the East Asian sector, it is surprising that higher CEJ intensity was seen in the East Asian sector (~−32 nT) when compared to that one seen in the African sector (~−9 nT) around day 71. However, in most cases, we found that the higher the value of the tidal component, the higher the CEJ intensity. This is glaring in the American sector where a CEJ intensity reaches ~−43 nT (around day 42, Figure 4a) and ~−42 nT (around day 57, Figure 4b) and its corresponding tidal component value was ~19 and ~−18 nT during the 2005/2006 and 2008/2009 SSW events, respectively.

Another supporting evidence, which confirms that changes in the value of a tidal component can be linked to CEJ intensity, was revealed in the East Asian sector during the 2008/2009 SSW event (Figure 5d). Clearly, around day 71 in the East Asian sector, which was after the 2008/2009 SSW event was subsiding, the highest value of a lunar semidiurnal tidal component reaches ~ 6 nT (Figure 5d) and the highest CEJ intensity was ~ −32 nT (Figure 4d). In comparison to the one near the peak of the reversing *U*, the highest value of a lunar semidiurnal tidal component was ~8 nT (Figure 5d) and the highest CEJ intensity was ~−42 nT. Now, in the context of the frequency of CEJ occurrence, it is surprising to note that the higher value of a tidal component seems irrelevant. For example, the frequency of CEJ occurrence that persisted for a longer period (~12 days) in the East Asian sector during the 2008/2009 SSW event (Figure 4d) is seen for a short time (~8 days) in the American sector during both SSW events (Figures 4a and 4b). These clearly revealed that increase in occurrence and magnitude of CEJ were obvious in our results during both SSW events compared to their precondition periods. This is due to minor and major warming characteristics that are lacking during the precondition periods of both SSW events. This is because upward propagating waves during the precondition periods were either filtered out in the lower atmosphere or not sufficient to make strong modulation to any of the tidal components at mesospheric altitudes.

Another school of thought suggested by Randel et al. (2002) is that the meridional circulation associated with SSW can induce upwelling in the equatorial region and produce cooling in the equatorial lower stratosphere while modifying the distribution of minor constituents. With these explanations above, the reality is that the stratospheric background wind during the precondition periods is not expected to exhibit any significant change that could prolong a CEJ event. Surprisingly, a prolonged period of CEJ occurrence that begins during the precondition of the 2005/2006 SSW gets reduced around days 41–46 and ends when the SSW was ongoing characterized the African sector. This is a confirmation that it is not only during the SSW-induced periods that a CEJ event can be prolonged. It is also a manifestation that the background wind during the precondition period in the African sector can sustain CEJ and prolong it. The wind system during the SSW events has revealed significant changes in the semidiurnal solar phase in all the sectors during the SSW events (Figures 7 and 8). The semidiurnal lunar phase in EEJ strength shows no variation when *U* was reversing. In addition, during the SSW, there is a steady decrease in the solar semidiurnal phase toward the later hour when the effect of the SSW is intense, which brings about significant reduction in EEJ strength and CEJ intensity in the East Asian and African sectors (Figure 7). For the lunar semidiurnal phase, our results show its typical propagation in solar time, but in the Asian sector, the phase value seems to be perturbed when *U* was reversing during the 2008/2009 SSW event. Similar slight perturbation is evident in the African sector after *U* had reversed (Figure 8f).

The brief reduction in ionospheric current seen at PST (a southern middle-latitude station) in our results after the reversal of *U* was similar to the changes reported in the horizontal geomagnetic field (ΔH) investigated by Yamazaki, Yumoto, et al. (2012), which were attributed to a westward current. An expected and consistent eastward current around noon time before the SSW begins that later on changed to westward current after *U* had reversed was obvious at KOU, a low-latitude station. Surprisingly, there is no significant change in the equivalent ionospheric current at FRN (a northern middle-latitude station) during and after *U* had reversed. This singularity in the physical mechanism observed in the ionospheric current during

both SSW events may be associated with wind-driven ionospheric dynamo or with a varying conductivity, the geomagnetic main field, and other *E*-layer features. Yamazaki, Richmond, et al. (2012) remarked that the solar antisymmetric (2, 3) semidiurnal modes from below ionosphere play a significant role in the dynamo current system oscillations during the SSW event. In addition to solar tidal modes, several studies have highlighted the semidiurnal lunar tide variation as the major driver of the equatorial and low-/middle-latitude dynamics (Maute et al., 2016). The interactions between tides, gravity, and planetary waves play a major role in ionospheric variability during the SSW event (Pedatella et al., 2016).

5. Conclusions

We have studied and compared the global magnetic daily variations during the 2005/2006 and 2008/2009 SSW events using magnetic field records obtained from the American, East Asian-Australian, and European-African sectors. The main results are given as follows:

1. The strength of the enhancement in EEJ current is associated with the duration of the reversed mean zonal wind in the stratosphere across all the sectors.
2. The significant CEJ occurrence associated with significant enhancement in EEJ current occurred in all of the stations during the 2005/2006 SSW event. In comparison to the well-investigated 2008/2009 SSW event, the similar feature appeared in all of the sectors when the westward zonal mean wind attained its maximum during the SSW.
3. CEJ occurrence is obvious during the SSW-induced period compared to the precondition period.
4. The changes in the lunar semidiurnal tidal components are observed with the significant enhancement in EEJ strength when it is not associated with the CEJ current.
5. Daily tidal components prior to and after both SSW events are high, moderate, and low in the American, East Asian, and African sectors, respectively. This is in accordance with EEJ intensities in the American sector during both SSW events being significantly compared to EEJ intensities observed in the East Asian and African sectors when SSW events are not evolving.
6. There are no significant perturbations in the equivalent ionospheric current due to SSW at middle-latitude stations. However, a significant reduction in ionospheric current was obvious after the zonal wind reverses in the stratosphere during both SSW events at a low-latitude station.

In principle, our results have revealed the possible factors that could be responsible for strong longitudinal difference in the dynamics of equatorial ionosphere. The ionospheric current system may be associated with a tidal effect caused by changes in the wind and temperature fields. Further investigations are needed for a deeper insight into the dynamic and electrodynamic forcing associated with the equatorial-ionosphere-thermosphere system during the SSW events.

Acknowledgments
This work was supported by the National Natural Science Foundation of China (41831070 and 41325017), and the Open Research Project of Large Research Infrastructures of CAS —"Study on the Interaction Between Low/Mid-Latitude Atmosphere and Ionosphere Based on the Chinese Meridian Project." C. Owolabi is grateful to the Chinese Scholarship Council (CSC) for making the CSC scholarship possible for his doctoral studies. The authors are very grateful to the INTERMAGNET (http://www.intermagnet.org), WDC (http://www.wdc.bgs.ac.uk/data.html), MAGDAS/CPMN (http://data.icswse.kyushu-u.ac.jp), OHP (http://ohpdmc.eri.u-tokyo.ac.jp), and JMA ((https://www.jma.go.jp/jma/indexe.html) teams for providing records of geomagnetic data used in this study. We are very thankful to IAGA (http://www.geomag.bgs.ac.uk/cgi-bin/coordcalc) for providing a quasi-dipole geomagnetic coordinate calculator. We are very grateful to the NCEP/NCAR reanalysis team for providing access to the zonal mean zonal wind and stratospheric temperature data set used in this study. Thanks are due to the Atmospheric Chemistry and Dynamics Laboratory at National Aeronautics and Space Administration (NASA)/GSFC for providing the zonal wave numbers data in geopotential height used in this study. We thank the SPDF/GSFC for providing record of *Kp* index and daily $F_{10.7}$ solar radio flux data used in the present study (https://omniweb.gsfc.nasa.gov/form/dx1.html).

References

Abdu, M. A., Batista, I. S., Carrasco, A. J., & Brum, C. G. M. (2005). South Atlantic magnetic anomaly ionization: A review and a new focus on electrodynamic effects in the equatorial ionosphere. *Journal of Atmospheric and Solar-Terrestrial Physics*, *67*(17-18), 1643–1657. https://doi.org/10.1016/j.jastp.2005.01.014

Abdu, M. A., Batista, P. P., Batista, I. S., Brum, C. G. M., Carrasco, A. J., & Reinisch, B. W. (2006). Planetary wave oscillations in mesospheric winds, equatorial evening prereversal electric field and spread F. *Geophysical Research Letters*, *33*, L07107. https://doi.org/10.1029/2005GL024837

Anderson, D., Anghel, A., Chau, J., & Veliz, O. (2004). Daytime vertical $\mathbf{E} \times \mathbf{B}$ drift velocities inferred from ground-based magnetometer observations at low latitudes. *Space Weather*, *2*, S11001. https://doi.org/10.1029/2004SW000095

Andrews, D., Holton, J. R., & Leroy, C. B. (1987). *Middle atmosphere dynamics* (pp. 259–294). London: Academic.

Beard, A. G., Mitchell, N. J., Williams, P. J. S., & Kunitake, M. (1999). Non-linear interactions between tides and planetary waves resulting in periodic tidal variability. *Journal of Atmospheric and Solar-Terrestrial Physics*, *61*(5), 363–376. https://doi.org/10.1016/s1364-6826(99)00003-6

Bolaji, O. S., Oyeyemi, E. O., Owolabi, O. P., Yamazaki, Y., Rabiu, A. B., Okoh, D., et al. (2016). Solar quiet current response in the African sector due to a 2009 sudden stratospheric warming event. *Journal of Geophysical Research: Space Physics*, *121*, 8055–8065. https://doi.org/10.1002/2016JA022857

Campbell, W. H., Arora, B. R., & Schiffmacher, E. R. (1993). External Sq currents in the India-Siberia region. *Journal of Geophysical Research*, *98*(A3), 3741–3752. https://doi.org/10.1029/92ja02552

Chapman, S., & Bartels, J. (1940). *Geomagnetism*, vols. 1 and 2. New York: Oxford University Press.

Charlton, A. J., & Polvani, L. M. (2007). A new look at stratospheric sudden warmings. Part I: Climatology and modeling benchmarks. *Journal of Climate*, *20*(3), 449–469. https://doi.org/10.1175/jcli3996.1

Chau, J. L., Aponte, N. A., Cabassa, E., Sulzer, M. P., Goncharenko, L. P., & González, S. A. (2010). Quiet time ionospheric variability over Arecibo during sudden stratospheric warming events. *Journal of Geophysical Research*, *115*, A00G06. https://doi.org/10.1029/2010JA015378

Chau, J. L., Hoffmann, P., Pedatella, N. M., Matthias, V., & Stober, G. (2015). Upper mesospheric lunar tides over middle and high latitudes during sudden stratospheric warming events. *Journal of Geophysical Research: Space Physics*, *120*, 3084–3096. https://doi.org/10.1002/2015JA020998

Doumouya, V., Cohen, Y., Arora, B., & Yumoto, K. (2003). Local time and longitude dependence of the equatorial electrojet magnetic effects. *Journal Atmospheric and Solar-Terrestrial Physics*, *65*(14-15), 1265–1282. https://doi.org/10.1016/j.jastp.2003.08.014

Emmert, J. T., Richmond, A. D., & Drob, D. P. (2010). A computationally compact representation of Magnetic-Apexand Quasi-Dipole coordinates with smooth base vectors. *Journal of Geophysical Research*, *115*, A08322. https://doi.org/10.1029/2010JA015326

Fejer, B. G., Olson, M. E., Chau, J. L., Stolle, C., Lühr, H., Goncharenko, L. P., et al. (2010). Lunar dependent equatorial ionospheric electrodynamics effects during sudden stratospheric warmings. *Journal of Geophysical Research*, *115*, A00G03. https://doi.org/10.1029/2010JA015273

Forbes, J. M. (1981). The equatorial electrojet. *Reviews of Geophysics*, *19*(3), 469. https://doi.org/10.1029/rg019i003p00469

Forbes, J. M., Zhang, X., Palo, S., Russell, J., Mertens, C. J., & Mlynczak, M. (2008). Tidal variability in the ionospheric dynamo region. *Journal of Geophysical Research*, *113*, A02310. https://doi.org/10.1029/2007JA012737

Goncharenko, L. P., Chau, J. L., Liu, H.-L., & Coster, A. J. (2010). Unexpected connections between the stratosphere and ionosphere. *Geophysical Research Letters*, *37*, L10101. https://doi.org/10.1029/2010GL043125

Goncharenko, L. P., Coster, A. J., Chau, J. L., & Valladares, C. E. (2010). Impact of sudden stratospheric warmings on equatorial ionization anomaly. *Journal of Geophysical Research*, *115*, A00G07. https://doi.org/10.1029/2010JA015400

Hagan, M. E., & Forbes, J. M. (2002). Migrating and nonmigrating diurnal tides in the middle and upper atmosphere excited by tropospheric latent heat release. *Journal of Geophysical Research*, *107*(D24), 4754. https://doi.org/10.1029/2001JD001236

Hagan, M. E., & Roble, R. G. (2001). Modeling diurnal tidal variability with the National Center for Atmospheric Research thermosphere-ionosphere-mesosphere-electrodynamics general circulation model. *Journal of Geophysical Research*, *106*(A11), 24,869–24,882. https://doi.org/10.1029/2001ja000057

Kalnay, E., Kanamitsu, M., Kistler, R., Collins, W., Deaven, D., Gandin, L., et al. (1996). The NCEP/NCAR 40-year reanalysis project. *Bulletin of the American Meteorological Society*, *77*(3), 437–471. https://doi.org/10.1175/1520-0477(1996)077<0437:TNYRP>2.0.CO;2

Kerridge, D. J. (2001). INTERMAGNET: Worldwide near-real-time geomagnetic observatory data. Proceeding of the European Space Agency Space Weather Workshop, European Space Research and Technology Centre, Noordwijk, Netherlands. Retrieved from www.intermagnet.org/publications/IM_ESTEC.pdf

Lindzen, R., & Chapman, S. (1969). Atmospheric tides. *Space Science Reviews*, *10*(1). https://doi.org/10.1007/bf00171584

Liu, H.-L., & Roble, R. G. (2002). A study of a self-generated stratospheric sudden warming and its mesospheric impacts using the coupled TIME-GCM/CCM3. *Journal of Geophysical Research*, *107*(D23), 4695. https://doi.org/10.1029/2001JD001533

Liu, H.-L., & Roble, R. G. (2005). Dynamical coupling of the stratosphere and mesosphere in the 2002 Southern Hemisphere major stratospheric sudden warming. *Geophysical Research Letters*, *32*, L13804. https://doi.org/10.1029/2005GL022939

Liu, H.-L., Talaat, E. R., Roble, R. G., Lieberman, R. S., Riggin, D. M., & Yee, J. H. (2004). The 6.5 day wave and its seasonal variability in the middle and upper atmosphere. *Journal of Geophysical Research*, *109*, D21112. https://doi.org/10.1029/2004JD004795

Love, J. J., & Gannon, J. L. (2009). Revised Dst and the epicycles of magnetic disturbance: 1958–2007. *Annales Geophysicae*, *27*(8), 3101–3131. https://doi.org/10.5194/angeo-27-3101-2009

Manney, G. L., Krüger, K., Pawson, S., Minschwaner, K., Schwartz, M. J., Daffer, W. H., et al. (2008). The evolution of the stratopause during the 2006 major warming: Satellite data and assimilated meteorological analyses. *Journal of Geophysical Research*, *113*, D11115. https://doi.org/10.1029/2007JD009097

Manoj, C., Lühr, H., Maus, S., & Nagarajan, N. (2006). Evidence for short spatial correlation lengths of the noontime equatorial electrojet inferred from a comparison of satellite and ground magnetic data. *Journal of Geophysical Research*, *111*, A11312. https://doi.org/10.1029/2006ja011855

Matsushita, S., & Xu, W.-Y. (1984). Seasonal variations of *L* equivalent current systems. *Journal of Geophysical Research*, *89*(A1), 285–294. https://doi.org/10.1029/ja089ia01p00285

Maute, A., Fejer, B. G., Forbes, J. M., Zhang, X., & Yudin, V. (2016). Equatorial vertical drift modulation by the lunar and solar semidiurnal tides during the 2013 sudden stratospheric warming. *Journal of Geophysical Research: Space Physics*, *121*, 1658–1668. https://doi.org/10.1002/2015ja022056

Maute, A., Hagan, M. E., Richmond, A. D., & Roble, R. G. (2014). TIME-GCM study of the ionospheric equatorial vertical drift changes during the 2006 stratospheric sudden warming. *Journal of Geophysical Research: Space Physics*, *119*, 1287–1305. https://doi.org/10.1002/2013ja019490

Maute, A., Hagan, M. E., Yudin, V., Liu, H.-L., & Yizengaw, E. (2015). Causes of the longitudinal differences in the equatorial vertical $E \times B$ drift during the 2013 SSW period as simulated by the TIME-GCM. *Journal of Geophysical Research: Space Physics*, *120*, 5117–5136. https://doi.org/10.1002/2015JA021126

Maute, A., Richmond, A. D., & Roble, R. G. (2012). Sources of low-latitude ionospheric $\mathbf{E} \times \mathbf{B}$ drifts and their variability. *Journal, of Geophysical Research*, *117*, A06312. https://doi.org/10.1029/2011JA017502

Mitchell, N. J., Middleton, H. R., Beard, A. G., Williams, P. J. S., & Muller, H. G. (1999). The 16-day planetary wave in the mesosphere and lower thermosphere. *Annales Geophysicae*, *17*(11), 1447–1456. https://doi.org/10.1007/s00585-999-1447-9

Pancheva, D., Mukhtarov, P., Andonov, B., Mitchell, N. J., & Forbes, J. M. (2009). Planetary waves observed by TIMED/SABER in coupling the stratosphere–mesosphere–lower thermosphere during the winter of 2003/2004: Part 2—Altitude and latitude planetary wave structure. *Journal of Atmospheric and Solar-Terrestrial Physics*, *71*(1), 75–87. https://doi.org/10.1016/j.jastp.2008.09.027

Pandey, K., Sekar, R., Anandarao, B. G., Gupta, S. P., & Chakrabarty, D. (2018). On the occurrence of afternoon counter electrojet over Indian longitudes during June solstice in solar minimum. *Journal of Geophysical Research: Space Physics*. https://doi.org/10.1002/2017JA024725

Patra, A. K., Pavan Chaitanya, P., Sripathi, S., & Alex, S. (2014). Ionospheric variability over Indian low latitude linked with the 2009 sudden stratospheric warming. *Journal of Geophysical Research: Space Physics*, *119*, 4044–4061. https://doi.org/10.1002/2014JA019847

Pedatella, N., Chau, J., Schmidt, H., Goncharenko, L., Stolle, C., Hocke, K., et al. (2018). How sudden stratospheric warming affects the whole atmosphere. *Eos*, *99*. https://doi.org/10.1029/2018EO092441

Pedatella, N. M., Fang, T.-W., Jin, H., Sassi, F., Schmidt, H., Chau, J. L., et al. (2016). Multimodel comparison of the ionosphere variability during the 2009 sudden stratosphere warming. *Journal of Geophysical Research: Space Physics*, *121*, 7204–7225. https://doi.org/10.1002/2016JA022859

Pedatella, N. M., & Forbes, J. M. (2010). Evidence for stratosphere sudden warming-ionosphere coupling due to vertically propagating tides. *Geophysical Research Letters*, *37*, L11104. https://doi.org/10.1029/2010GL043560

Pedatella, N. M., Forbes, J. M., & Richmond, A. D. (2011). Seasonal and longitudinal variations of the solar quiet (*Sq*) current system during solar minimum determined by CHAMP satellite magnetic field observations. *Journal of Geophysical Research*, *116*, A04317. https://doi.org/10.1029/2010JA016289

Pogoreltsev, A. I., Vlasov, A. A., Fröhlich, K., & Jacobi, C. (2007). Planetary waves in coupling the lower and upper atmosphere. *Journal of Atmospheric and Solar-Terrestrial Physics*, *69*(17-18), 2083–2101. https://doi.org/10.1016/j.jastp.2007.05.014

Randel, W., Chanin, M. L., & Michaut, C. (2002). SPARC intercomparison of middle atmosphere climatologies, SPARC, WCRP 96, WMO/TD, No. 1142; SPARC Report No. 3.

Richmond, A. D. (1995). Ionospheric electrodynamics using magnetic apex coordinates. *Journal of Geomagnetism and Geoelectricity*, *47*(2), 191–212. https://doi.org/10.5636/jgg.47.191

Richmond, A. D., & Lu, G. (2000). Upper-atmospheric effects of magnetic storms: A brief tutorial. *Journal Atmospheric and Solar-Terrestrial Physics*, *62*(12), 1115–1127. https://doi.org/10.1016/S1364-6826(00)00094-8

Rishbeth, H., & Mendillo, M. (2001). Patterns of F2-layer variability. *Journal of Atmospheric and Solar-Terrestrial Physics*, *63*(15), 1661–1680 . https://doi.org/10.1016/s1364-6826(01)00036-0

Sathishkumar, S., & Sridharan, S. (2013). Lunar and solar tidal variabilities in mesospheric winds and EEJ strength over Tirunelveli (8.7°N, 77.8°E) during the 2009 major stratospheric warming. *Journal of Geophysical Research: Space Physics*, *118*, 533–541. https://doi.org/10.1029/2012ja018236

Sathishkumar, S., Sridharan, S., & Jacobi, C. (2009). Dynamical response of low-latitude middle atmosphere to major sudden stratospheric warming events. *Journal Atmospheric and Solar-Terrestrial Physics*, *71*(8-9), 857–865. https://doi.org/10.1016/j.jastp.2009.04.002

Siddiqui, T. A., Maute, A., Pedatella, N., Yamazaki, Y., Lühr, H., & Stolle, C. (2018). On the variability of the semidiurnal solar and lunar tides of the equatorial electrojet during sudden stratospheric warmings. *Annales Geophysicae Discussions*, *1–24*, 1–24. https://doi.org/10.5194/angeo-2018-80

Soares, G., Yamazaki, Y., Matzka, J., Pinheiro, K., Morschhauser, A., Stolle, C., & Alken, P. (2018). Equatorial counter electrojet longitudinal and seasonal variability in the American sector. *Journal of Geophysical Research: Space Physics*, *123*, 9906–9920. https://doi.org/10.1029/2018JA025968

Sridharan, S., Gurubaran, S., & Rajaram, R. (2002). Structural changes in the tidal components in mesospheric winds as observed by the MF radar during afternoon counter electrojet events. *Journal Atmospheric and Solar-Terrestrial Physics*, *64*(12-14), 1455–1463. https://doi.org/10.1016/S1364-6826(02)00109-8

Stening, R. J. (1989). A calculation of ionospheric currents due to semidiurnal asymmetric tides. *Journal of Geophysical Research*, *94*(A2), 1525–1531. https://doi.org/10.1029/ja094ia02p01525

Stening, R. J., Meek, C. E., & Manson, A. H. (1996). Upper atmosphere wind systems during reverse equatorial electrojet events. *Geophysical Research Letters*, *23*(22), 3243–3246. https://doi.org/10.1029/96gl02611

Sugiura, M., & Fanselau, G. (1966). Lunar phase numbers ν and ν' for years 1850 to 2050. (Report X-612-66-401). Prepared in part for the IAGA-IAMAP Joint Committee on Lunar Effects, Greenbelt, MD: Goddard Space Flight Center.

Takeda, M. (1999). Time variation of global geomagnetic Sq field in 1964 and 1980. *Journal Atmospheric and Solar-Terrestrial Physics*, *61*(10), 765–774. https://doi.org/10.1016/S1364-6826(99)00028-0

Takeda, M., & Araki, T. (1984). Ionospheric currents and fields during the solar eclipse. *Planetary and Space Science*, *32*(8), 1013–1019. https://doi.org/10.1016/0032-0633(84)90057-6

Toh, H., Hamano, Y., & Ichiki, M. (2006). Long-term seafloor geomagnetic station in the northwest Pacific: A possible candidate for a seafloor geomagnetic observatory. *Earth, Planets and Space*, *58*(6), 697–705. https://doi.org/10.1186/BF03351970

Vineeth, C., Kumar Pant, T., & Sridharan, R. (2009). Equatorial counter electrojets and polar stratospheric sudden warmings—A classical example of high latitude-low latitude coupling. *Annales Geophysicae*, *27*(8), 3147–3153. https://doi.org/10.5194/angeo-27-3147-2009

Vineeth, C., Pant, T. K., Devasia, C. V., & Sridharan, R. (2007). Highly localized cooling in daytime mesopause temperature over the dip equator during counter electrojet events: First results. *Geophysical Research Letters*, *34*, L14101. https://doi.org/10.1029/2007GL030298

Vineeth, C., Pant, T. K., & Hossain, M. M. (2012). Enhanced gravity wave activity over the equatorial MLT region during counter electrojet events. *Indian Journal of Space and Radio Physics*, *41*, 258–263.

Weimer, D. R. (2013). An empirical model of ground-level geomagnetic perturbations. *Space Weather*, *11*, 107–120. https://doi.org/10.1002/swe.20030

Yacob, A. (1977). Internal induction by the equatorial electrojet in India examined with surface and satellite geomagnetic observations. *Journal of Atmospheric and Solar-Terrestrial Physics*, *39*(5), 601–606. https://doi.org/10.1016/0021-9169(77)90070-8

Yamazaki, Y., & Maute, A. (2016). Sq and EEJ—A Review on the Daily Variation of the Geomagnetic Field Caused by Ionospheric Dynamo Currents. *Space Science Reviews*, *206*(1-4), 299–405. https://doi.org/10.1007/s11214-016-0282-z

Yamazaki, Y., Richmond, A. D., Liu, H.-L., Yumoto, K., & Tanaka, Y. (2012). Sq current system during stratospheric sudden warming events in 2006 and 2009. *Journal of Geophysical Research*, *117*, A12313. https://doi.org/10.1029/2012JA018116

Yamazaki, Y., Yumoto, K., Cardinal, M. G., Fraser, B. J., Hattori, P., Kakinami, Y., & Yoshikawa, A. (2011). An empirical model of the quiet daily geomagnetic field variation. *Journal of Geophysical Research*, *116*, A10312. https://doi.org/10.1029/2011JA016487

Yamazaki, Y., Yumoto, K., McNamara, D., Hirooka, T., Uozumi, T., Kitamura, K., et al. (2012). Ionospheric current system during sudden stratospheric warming events. *Journal of Geophysical Research*, *117*, A03334. https://doi.org/10.1029/2011JA017453

Yumoto, K., & the MAGDAS Group (2006). MAGDAS project and its application for space weather, Solar Influence on the Heliosphere and Earth's Environment. In N. Gopalswamy & A. Bhattacharyya (Eds.), *Recent Progress and Prospects* (pp. 309–405).

Zhou, Y.-L., Lühr, H., Xu, H.-W., & Alken, P. (2018). Comprehensive analysis of the counter equatorial electrojet: Average properties as deduced from CHAMP observations. *Journal of Geophysical Research: Space Physics*, *123*, 5159–5181. https://doi.org/10.1029/2018JA025526